KSCE Journal of Civil Engineering (2020) 24(4):1195-1208
DOI 10.1007/s12205-020-0671-4

pISSN 1226-7988, eISSN 1976-3808
www.springer.com/12205

Railroad Engineering

Mitigation of Temperature-Induced Curling of Concrete Roadbed along High-Speed Railway: In situ Experiment and Numerical Simulation

Yuan Yu[a,b], **Liang Tang**[a,b], **Xianzhang Ling**[a,c], **Degou Cai**[d], **Yangsheng Ye**[d], **and Lin Geng**[a,d]

[a]*School of Civil Engineering, Harbin Institute of Technology, Harbin 150090, China*
[b]*State Key Laboratory for Geomechanics and Deep Underground Engineering, Xuzhou 221008, China*
[c]*School of Civil Engineering, Qingdao University of Technology, Qingdao 266033, China*
[d]*Railway Engineering Research Institute, China Academy of Rails Science, Beijing 100081, China*

ARTICLE HISTORY

Received 21 April 2019
Revised 4 October 2019
Accepted 4 February 2020
Published Online 9 March 2020

KEYWORDS

Mitigation
Temperature-induced curling
Concrete roadbed
Finite element analysis
In situ monitoring test
High-speed railways

ABSTRACT

The concrete roadbed in the Beijing-Shenyang high-speed railway (HSR) is being serviced for the first time in HSR construction history. Rail inspections have shown that the extreme temperature conditions in seasonally freezing regions can significantly influence the curling behavior of concrete roadbeds. This paper presents an in situ experiment to fundamentally evaluate the impact of seasonal temperature variations on the curling behavior of concrete roadbeds. Herein, a thermomechanical coupled finite element (FE) model is built and calibrated with experimental data. Then, specific consideration is given to the curling mitigation measures, including adjusting the thickness, length, and construction form of the concrete roadbed. Mitigating upward-curling behavior by increasing the thickness of the concrete roadbed will result in severe downward-curling behavior during one year of service. Finally, an active groove-setting construction form is suggested to prevent curling from the temperature variations in the concrete roadbed. In general, this study further enhances the common understanding of the temperature curling behavior of concrete roadbeds serviced in an HSR.

1. Introduction

In China, 53.5% of the land area is seasonally freezing ground. The high-speed railway (HSR) construction in China is undergoing a revolution, and an HSR network is planned to be built in the seasonally freezing regions of China. Engineering practices and research have shown that frost heave and thawing settlement cause numerous highway roadbed damages in these regions. Therefore, soil susceptibility to frost heave is believed to be a major factor threatening the stability of roadbeds. To address this issue, the Beijing-Shenyang HSR was the first to adopt a concrete roadbed. This new type of concrete roadbed form is expected to be widely used in seasonally freezing regions due to the following advantages: frost heave prevention, lower maintenance costs, and increased durability.

All materials expand and shrink to some degree in response to temperature fluctuations (Sabih and Tarefder, 2016). When the surface of a concrete slab is hotter than the base, the upper part elongates more than lower part, causing the slab to curl upward (Armaghani et al., 1987). Early monitoring found a routine temperature-induced curling behavior on the concrete roadbed. Even if this phenomenon is negligible compared to the frost heave movement that occurred in the Harbin-Dalian HSR, this curling behavior may also result in track irregularity problems. This issue not only decreases riding comfort but also contributes to the potential of derailment in an HSR. Therefore, in-depth studies are needed to ensure the smoothness of concrete roadbeds.

In recent years, numerous researchers have conducted in situ experimental investigations to study the temperature conditions and the deformation behaviors of concrete slabs caused by alternating temperature conditions. Mohamed and Hansen (1997) found that the temperature gradient along the concrete slab depth is typically nonlinear. Yu et al. (1998) studied the temperature conditions of jointed plain concrete pavements and concluded that the fluctuation in temperature is greater on the surface of the slab than at the bottom of the slab. Bianchini (2013) identified the temperature difference between the top and bottom of the rigid pavement in Texas to evaluate the relationships between curling

CORRESPONDENCE Liang Tang hit_tl@163.com School of Civil Engineering, Harbin Institute of Technology, Harbin 150090, China; State Key Laboratory for Geomechanics and Deep Underground Engineering, Xuzhou 221008, China

trends and construction or curing techniques. Canga Ruiz et al. (2019) investigated the curling of rail transit concrete crossties due to temperature gradients. However, the curling behavior of the mass concrete roadbed built in the seasonally freezing region and relevant mitigation measures appear not to have been investigated to date.

Generally, the dimensions play a primary role in managing the tendency for temperature-induced curling behavior. There are some conflicting conclusions on the effect of slab thickness (Nam et al., 2014). Al Nasra and Wang (1994) reported that a thicker slab exhibits a greater curling movement, whereas Leonards and Harr (1959) stated that the upward corner movement decreases as the slab thickness increases. Such conflicting conclusions resulted because the former studies assumed either a fixed temperature differential regardless of slab thickness or a constant temperature increase per unit thickness, which do not account for the heat transport between the roadbed and the foundation. Suprenant (2002) revealed that in a finite slab (thickness less than 0.5 m), the slab length (joint spacing) has a substantial effect on the amount of curling; the amount of curling movement tended to decrease as the slab length decreased. As a new type of highway roadbed, a necessary attempt should be made to identify the influence of dimensions on the temperature-induced curling behavior of concrete roadbeds.

Significant recent research on finite element analysis of the thermal responses in concrete pavements, bridge girders, and concrete crossties can be found in the open literature (Mackiewicz, 2014; Zhu and Cai, 2014; Wolf et al., 2016; Mirza et al., 2016; Yang and Bradford, 2017). Ren et al. (2014) adopted a finite element method to determine the influence of the temperature gradient, adhesive strength, friction coefficient, terminal spine number, and terminal spine spacing on slab upwarping. Yang and Bradford (2017) parametrically investigated the thermal responses of concrete pavements by refined modeling, wherein the variables involved were imperfection amplitude, pavement weight and pavement stiffness. Nam et al. (2014) conducted a series of finite element (FE) simulations to review the effects of slab temperature conditions and other affecting parameters on the curling movements of jointed concrete pavements. To consider the effects of the built-in temperature gradient and nonlinear shrinkage gradient being reduced over time by creep in numerical modeling of concrete slabs, Rao and Roesler (2005) develop an approach to estimate the effective built-in temperature difference (EBITD) of concrete slabs through nondestructive testing. The concept of the EBITD is a cumulative effect of the built-in temperature gradient, shrinkage, and creep (e.g., Byrum, 2000; Beckemeyer et al., 2002; Hansen et al., 2002). The EBITD is a linear temperature difference between the top and the bottom of a concrete slab. In this study, the EBITD is used to consider the influence of differential drying shrinkage and creep in the mathematical model.

In the following sections, an in situ monitoring experiment is first presented, along with numerical simulation results. Based on the results, the temperature-induced curling behavior of concrete roadbeds is discussed. Finally, the related mitigation method is presented along with concluding remarks.

2. In situ Monitoring Experiment

An extensive measurement program is undertaken at the Kazuo

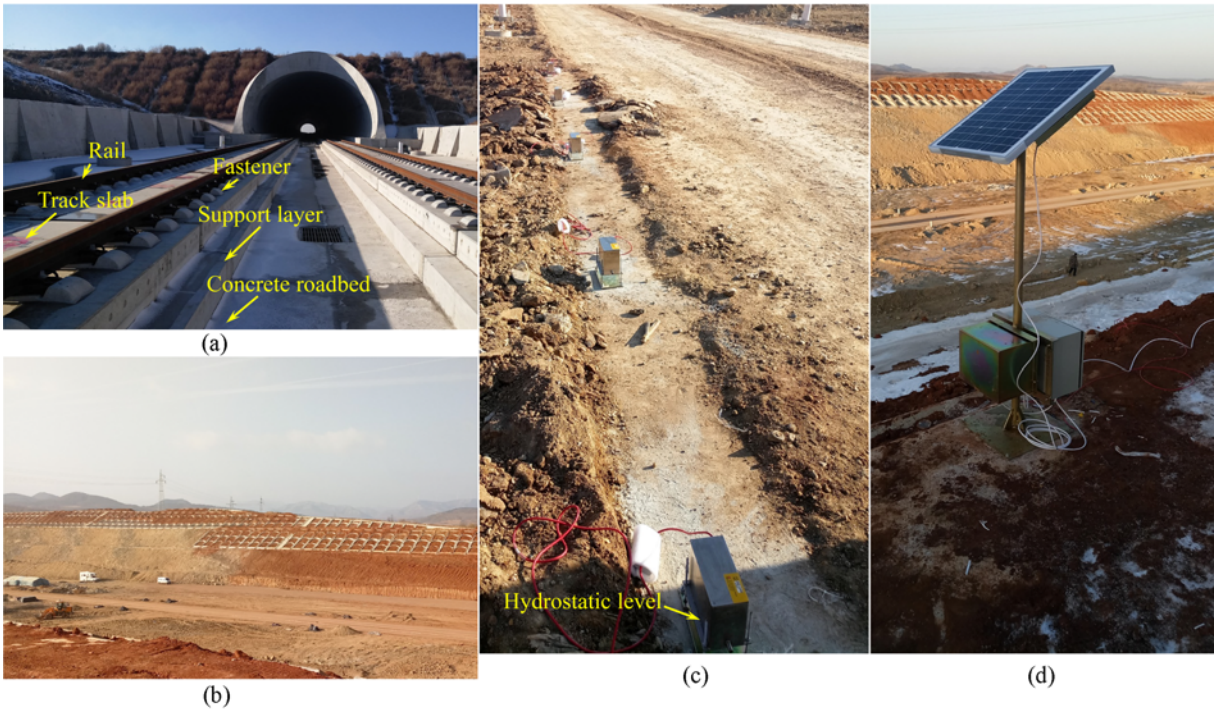

Fig. 1. In-situ Experiment at the Kazuo along Beijing-Shenyang High-Speed Railway: (a) DK347+250 – DK348+120 Section (completion), (b) DK347+250 – DK348+120 Section (under construction), (c) Hydrostatic Level System, (d) Data Acquisition System

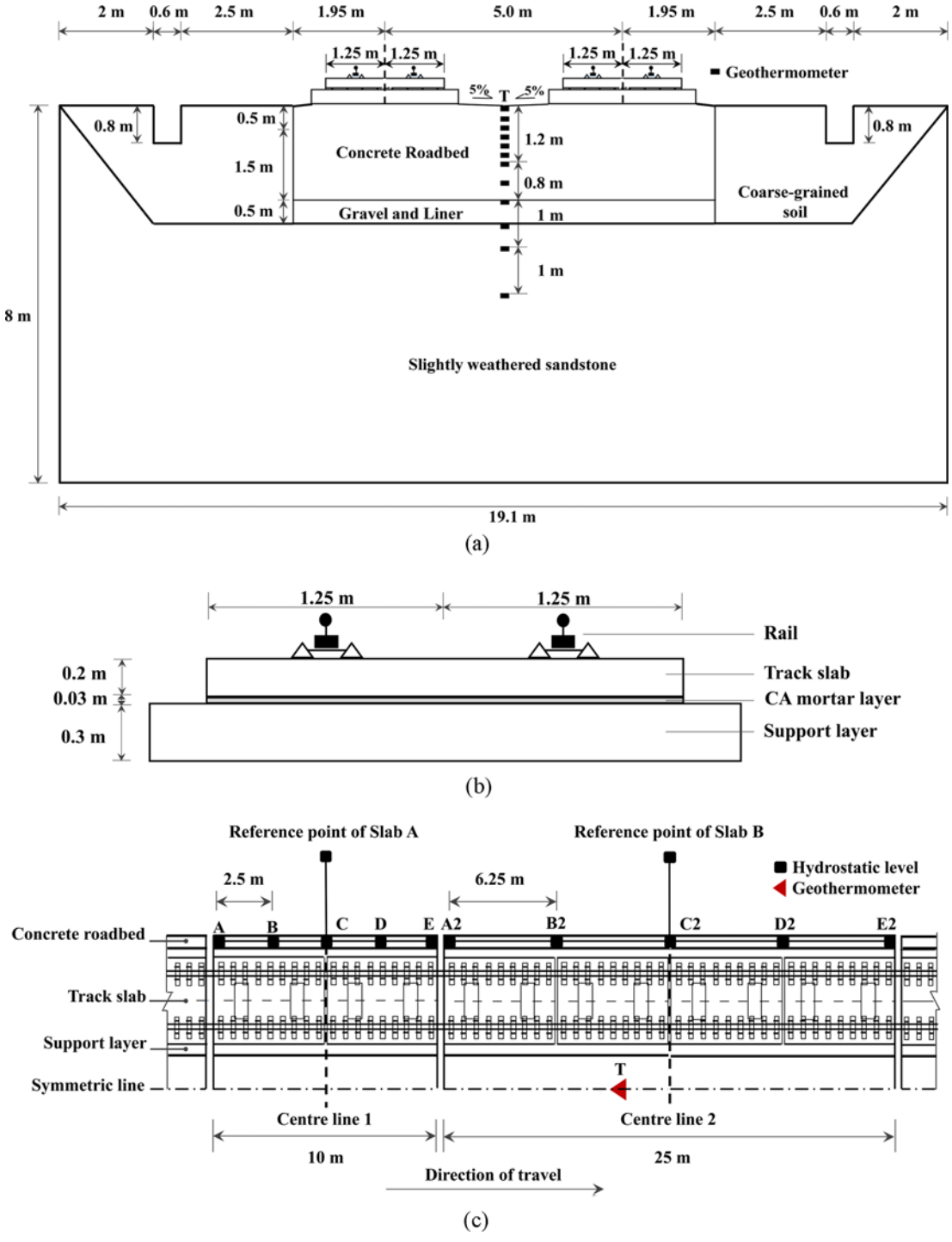

Fig. 2. Schematic of a Typical Track-Ground System along Beijing-Shenyang High-Speed Railway: (a) Cross-Section, (b) CRTS-II Slab Track, (c) Vertical View with Sensors Layout

section (i.e., DK347+250-DK349+543) along the Beijing-Shenyang HSR line (Fig. 1). A total of two in situ experiments with different roadbed length are performed. The thickness of both roadbeds is 2 m, and the lengths are 10 m and 25 m (Code for Design of High Speed Railway in China (TB 10621, 2014)). These two concrete roadbeds used in the experiment are adjacent to ensure a consistent test environment. The dimensions are used in the following studies. Moreover, the service status (i.e., temperature field and deformation) of the concrete roadbed has been recorded by a thermistor and hydrostatic level measuring (HLM) system.

Figures 2(a) – 2(c) presents a schematic of the typical track-ground system with the measurement portion. In this section, the freezing period occurs from November to March of the following

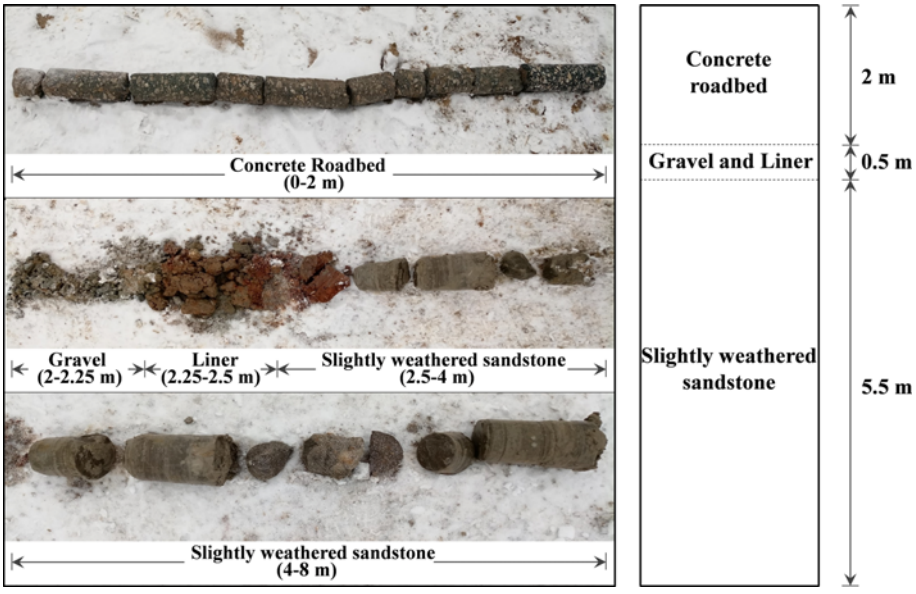

Fig. 3. Soil Samples of Monitoring Field

Table 1. Mechanical and Thermal Parameters of Materials (Parameter of CRTS-II slab track is obtained from Zhu and Cai, 2014.)

Materials	Elastic modulus, E (MPa)	Poisson's ratio, υ	Density, ρ (kg/m^3)	Thermal conductivity, λ [w/(m·°C)]	Specific heat, C [J/(kg·°C)]	Coefficient of thermal expansion, CTE (°C^{-1})	Tensile splitting strength, f_t (MPa)	Compressive strength, f'_c (MPa)
Concrete of roadbed	2.86×10^4	0.18	2,400	2.10	860	1.2×10^{-5}	3.60	43
Track slab in CRTS-II slab track	3.60×10^4	0.20	2,400	1.74	900	1.0×10^{-5}	-	-
CA mortar in CRTS-II slab track	8.00×10^3	0.20	2,400	0.93	800	1.5×10^{-5}	-	-
Support layer in CRTS-II slab track	2.55×10^4	0.20	2,400	1.00	830	1.5×10^{-5}	-	-
Coarse-grained soil	2.00×10^4	0.25	2,185	0.99	951	-	-	-
Gravel cushion	2.86×10^2	0.25	2,100	1.10	800	-	-	-
Slightly weathered sandstone	3.00×10^4	0.19	2,500	2.20	950	-	-	-

year. The temperature interval is approximately -29.9 to 42°C. Thus, each hydrostatic level measuring sensor is equipped with a temperature sensor, avoiding the influence of temperature on the measurement accuracy. Monitoring data are collected once an hour by a set of data acquisition systems with a solar photovoltaic module. As the section of the in situ experiments was not in operation during January 3 to May 12 in 2017, the influence from trains is negligible. Measurements and detailed discussion will be given in the next section.

According to the geotechnical investigations, the foundation can be characterized as slightly weathered sandstone (Fig. 3). Table 1 presents the key parameters of the roadbed concrete and the foundation along the Beijing-Shenyang HSR. The mechanical and thermal parameters of the CRTS-II slab track are obtained from the report of Zhu and Cai (2014). As the temperature of the foundation will not fall below zero (Fig. 5), the latent heat is not included in the following calculation model.

3. Numerical Investigations on Curling Behavior

All the FE simulations are conducted with ABAQUS 6.13 (2013). Numerical studies involve 1) forecasting temperature profiles along the depth of the concrete roadbed and 2) quantifying the curling behavior of the concrete roadbed.

3.1 Computational Formulation

Figure 4 shows the benchmark numerical model under investigation. The model of a concrete roadbed-foundation system is created in a Cartesian 3D system. Table 1 shows the parameters of the heat transport model. The slightly weathered sandstone foundation is modeled as an elastic support. Moreover, the slab track system is assumed to be purely elastic (Zhu and Cai, 2014).

The theoretical basis for the concrete damaged plasticity model used in this study is the yield function proposed by Lubliner et al. (1989). Moreover, Lee and Fenves (1998) made some revisions to this model to estimate the evolution of strength under tension and compression. The main parameters required for defining the plastic-damage model are the dilation angle (ψ), flow potential eccentricity (ε), initial biaxial compressive yield stress-to-initial uniaxial compressive yield stress ratio (fbo/fco), viscosity (μ), and strength ratio (K_c). The parameters above are given in Table 2.

A master-slave algorithm is used to define the interfacial

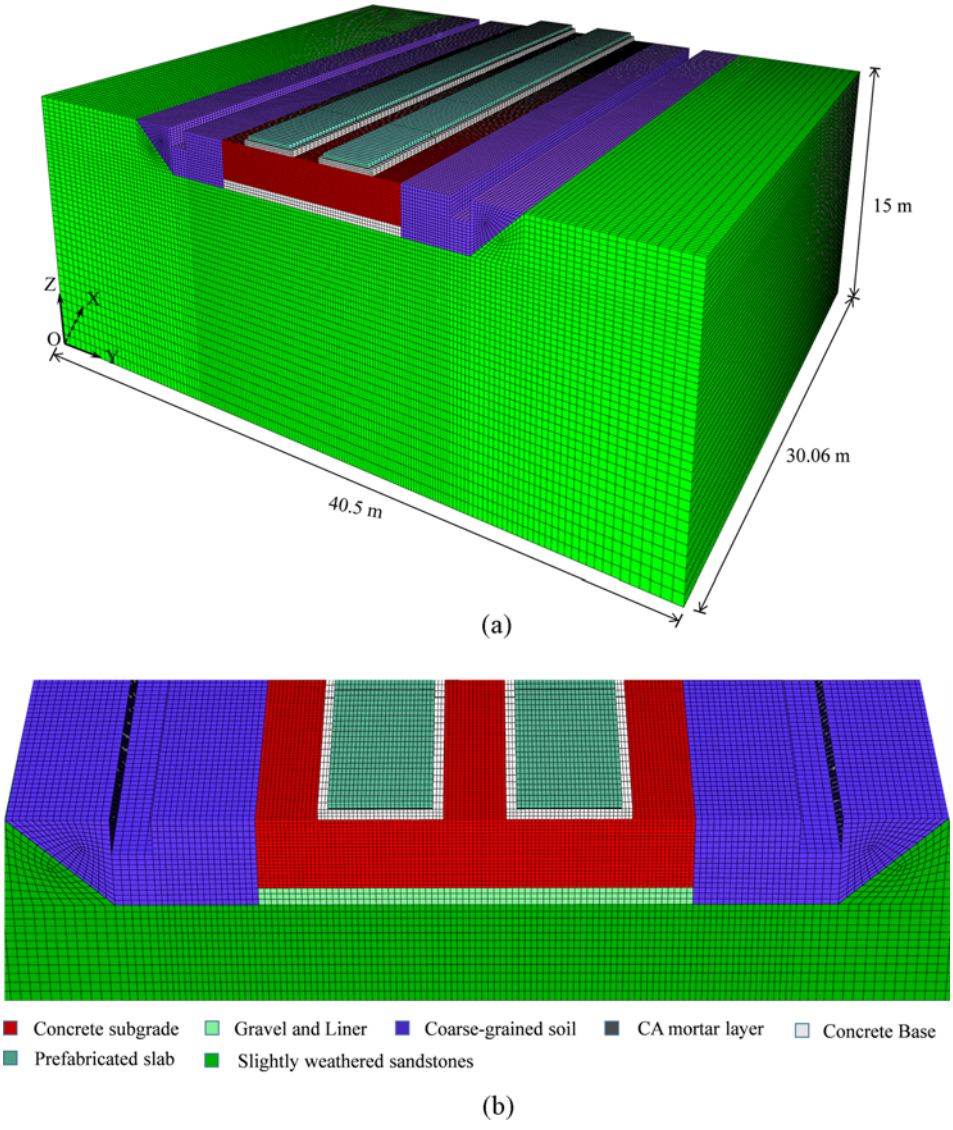

Fig. 4. Finite Element Modeling of Thermal-Stress Analysis: (a) Benchmark Model, (b) Detail Drawing

Table 2. Parameters Used in the Concrete Damaged Plasticity Model (after Genikomsou and Polak, 2015)

Materials	Dilation angle, ψ (°)	Flow potential eccentricity, ε	Stress ratio, f_{bo}/f_{co}	Viscosity parameter, μ	Shape factor, K_c
Concrete of roadbed	40	0.1	1.16	0.001	0.667

interactions. The sliding formulation is set as finite sliding. Recently, the friction coefficients at the interfaces for concrete-concrete bonds and concrete-soil bonds have been determined by many researchers (e.g., Mohamad et al., 2015; Canakci et al., 2016). On this basis, the stabilized coefficients of friction for the concrete roadbed-support layer contact and the concrete roadbed-coarse grained soil contact are set to 0.9 and 0.2, respectively.

The frictional behavior between the concrete roadbed and the gravel cushion is considered by defining the elastic slip and friction coefficient. This investigation assumes that the elastic slip is linear (Yang and Bradford, 2017) and that there is no heat transport in gaps wider than 1.5 mm. The parameters quantifying the elastic slip and the friction coefficient can be obtained from the test results through regression analysis (Jeong et al., 2014). In this study, the elastic slip is 0.6 mm, and the coefficient of friction is set to 0.7.

To consider the effects of shrinkage, creep, and built-in temperature gradient, the EBITD has been adopted in the predefined field. The range of the curling data over the 24 h cycle and the displacement relative to the first data point can be used to estimate the EBITD. By running a series of analyses with different EBITD values (0°C, -5°C, -10°C, -15°C, -20°C, -25°C, and -30°C), an estimate of the EBITD can be obtained by

matching the calculated and observed level of the curling data and the corner displacement. Finally, the EBITD is equal to -25°C in this study.

3.2 Temperature Model and Validation

The thermal boundary conditions are defined as follows: the temperature of the bottom is always 15°C and the lateral boundaries are adiabatic. Eq. (1) is used to simulate the surface boundary temperature, and the surface boundary temperature during January 3, 2017, to May 12, 2017, is replaced by the measured surface temperature of the concrete roadbed.

$$T_n = T_\alpha + \frac{\Delta T_w}{365}t + A\sin\left(\frac{2\pi t}{365} + \alpha_0\right) + \Delta T_F \quad (1)$$

where T_α = 3.5°C is the ground surface mean temperature, ΔT_w = 0.048°C represents the climate warming effect (Wei et al., 2011), t is the time (day), A = 19°C is the temperature amplitude at the natural ground surface, $\alpha_0 = \pi/2$ is the initial phase angle, and ΔT_F = 3.5°C represents the temperature increment caused by the adherent layer. Then, the initial temperature distribution is obtained through the in situ monitoring experiment.

To avoid the influence of the train and construction, measurements from January 3, 2017, to May 12, 2017, are used to verify the validity of the model. Fig. 5 displays the measured and computed mean temperature histories. The figure illustrates the remarkable decrease in the temperature gradient as the environment temperature rises. The predicted and measured temperature profiles are in close agreement. Additionally, the temperature fluctuation below a depth of 1.2 m is smaller than that in the upper part.

3.3 Mitigation Model and Validation

The displacement boundary condition is defined as follows: the

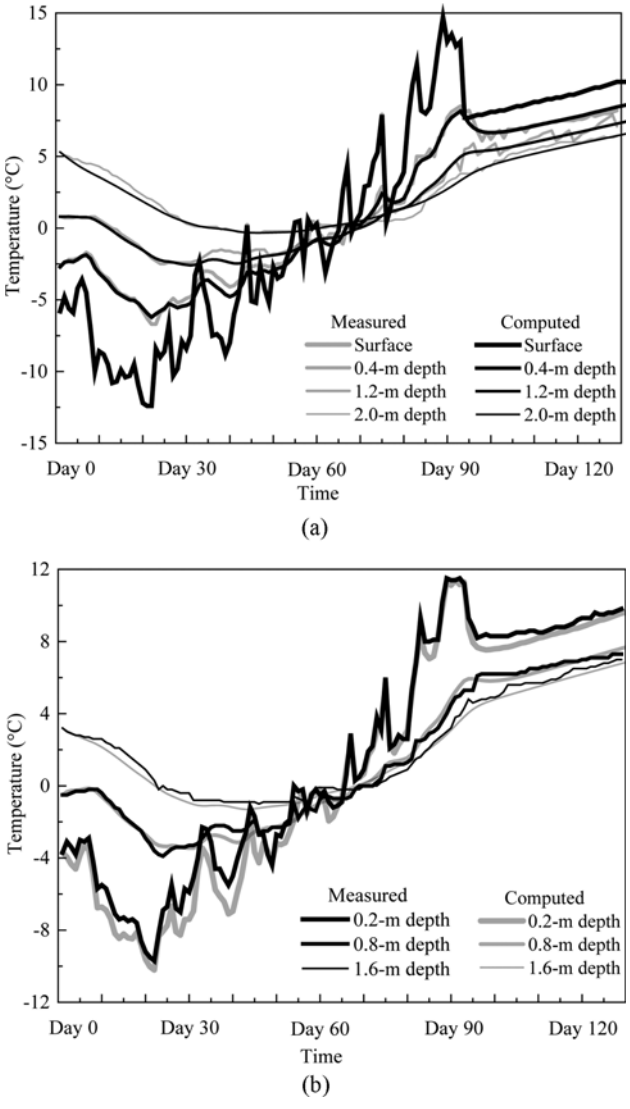

Fig. 5. Measured and Computed Mean Temperatures of Concrete Roadbed at Various Depths (time: from January 3rd, 2017 to May 12th, 2017): (a) Part I, (b) Part II (time: from January 3rd, 2017 to May 12th, 2017)

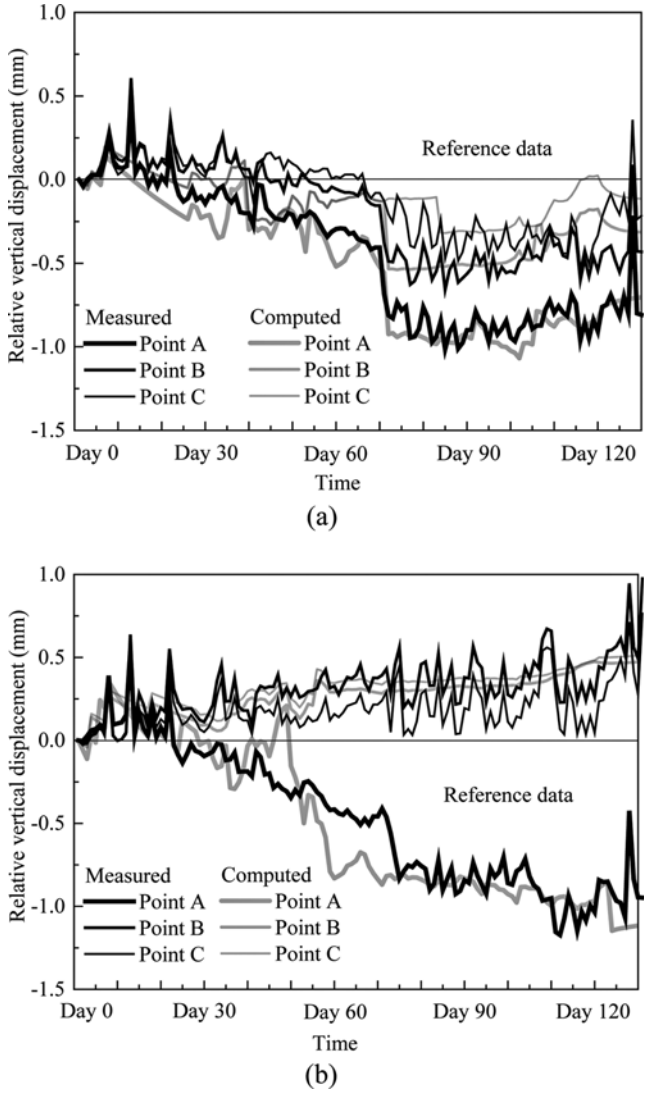

Fig. 6. Measured and Computed Relative Vertical Displacement of Concrete Roadbed during January 3rd to March 12th in 2017: (a) Slab Length =10 m, (b) Slab Length = 25 m

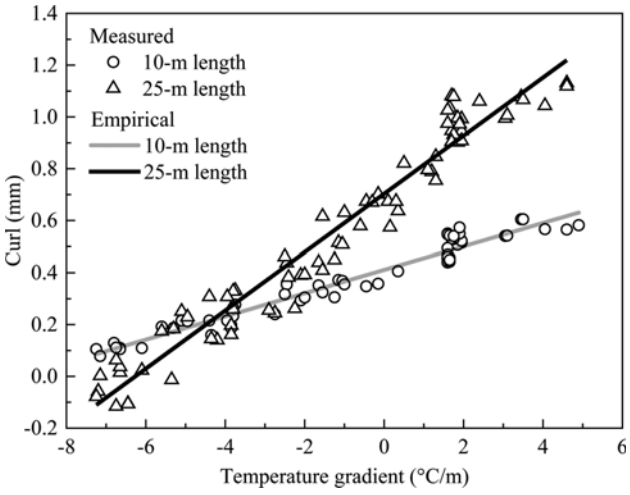

Fig. 7. Relationship between Curl and Temperature Gradient of Concrete Roadbed

lateral boundaries of the model are not allowed to move inward/outward and the bottom is restricted in all three directions. Moreover, the predefined field is the soil stress state obtained through the static application of gravity (own model weight).

Due to built-in curling, the first data of the hydrostatic level measuring system may not represent the actual condition of the concrete roadbed (Bianchini, 2013). Therefore, Fig. 6 presents the deformation relative to the first data point. As the surface temperature increases, the magnitude of the temperature gradient decreases (Fig. 5). Moreover, the upward-curling condition of the concrete roadbed turns into a downward-curling condition. The major downward deformation occurs on the corner of the concrete road, and the middle part moves up relative to the corner (Fig. 6).

To better quantify the curling behavior of the concrete roadbed, this study employs the curl documented by Wolf et al. (2016) in the longitudinal direction (direction of travel). The curl is calculated using Eq. (2).

$$f_{curl} = \delta_C - \frac{\delta_A + \delta_E}{2} \tag{2}$$

where δ_A, δ_C, and δ_E are the vertical deflections at points A, C, and E of the concrete roadbed, respectively (Fig. 2(c)). A positive curl indicates that the concrete roadbed is curling downward.

Figure 7 shows that there is a direct relationship between the curl and the temperature gradient. The curl varies approximately linearly with respect to the temperature gradient for both 25-m length and 10-m length concrete roadbeds. This empirical linear relationship presents a second method of predicting curling behavior. Eqs. (3) and (4) are used for the 10-m length and 25-m length concrete roadbeds, respectively:

$$f_{curl} = 0.04\Delta T + 0.41 \tag{3}$$

$$f_{curl} = 0.12\Delta T + 0.70 \tag{4}$$

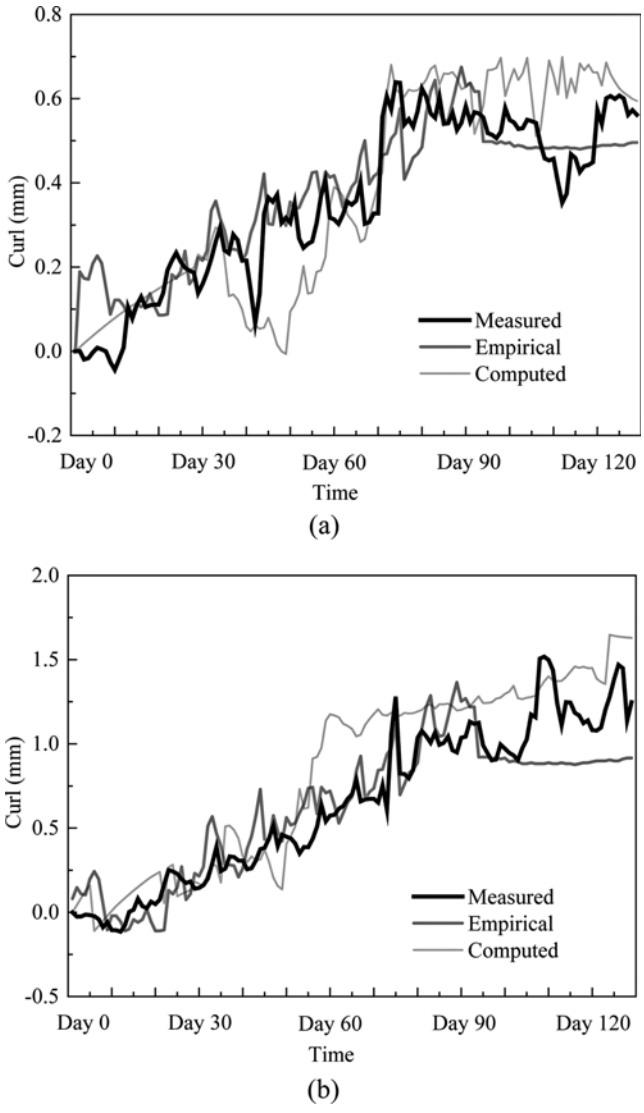

Fig. 8. Comparison of Empirical-Linear, Computed and Measured Curls of Concrete Roadbed: (a) Slab Length = 10 m, (b) Slab Length = 25 m

where ΔT_g = temperature gradient (°C/m).

Figure 8 presents a comparison between the measured, FEM computed, and empirical linear curl. The most significant error of the empirical linear curl is found to be 0.3 mm. These results show that the direct relationship is an effective means of estimating curling behavior. Moreover, the increase in roadbed length (10 m to 25 m) will lead to greater curling behavior under the same environmental conditions.

4. Parametric Analysis

One of the objectives of the in situ monitoring experiment was to build numerical models that can accurately simulate the observed temperature-induced curling behavior. Once validated, the model can be used to analyze the influence of numerous parameters and

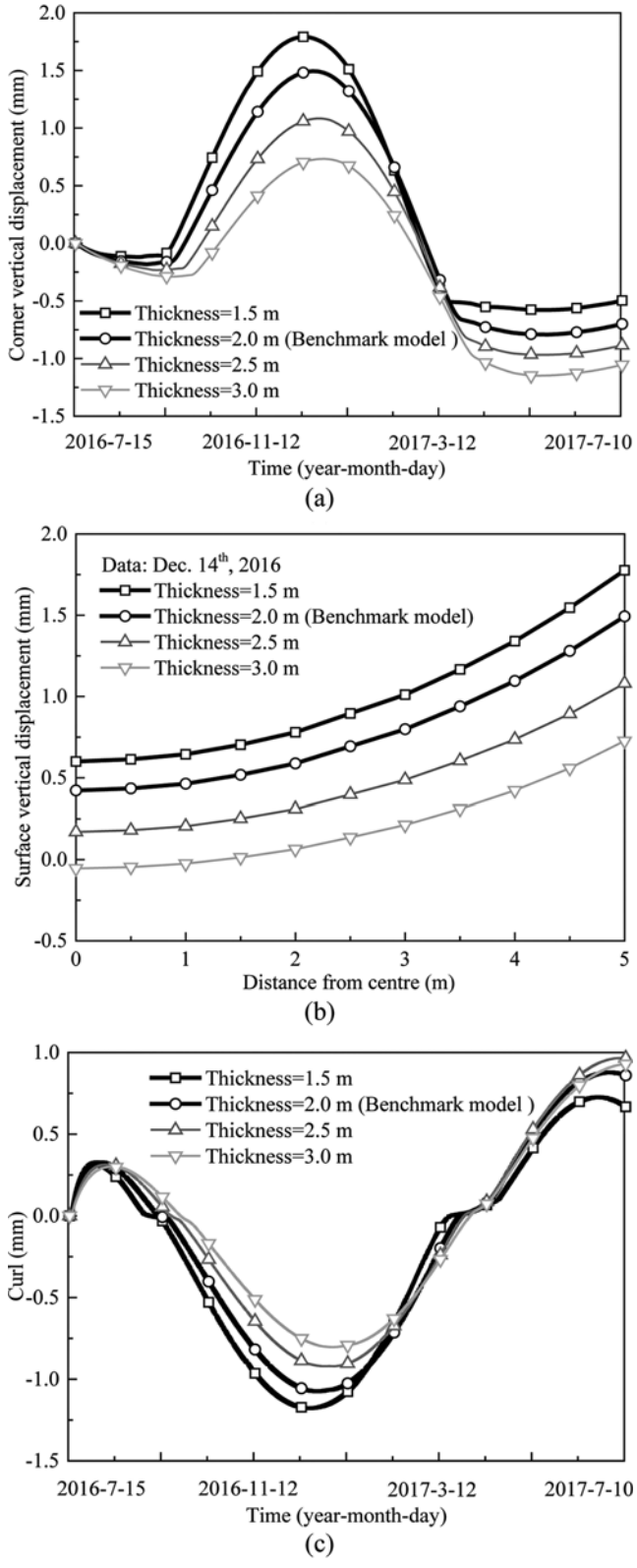

Fig. 9. Effect of Slab Thickness on the Deformation Behavior of the Concrete Roadbed: (a) Vertical Displacement at Roadbed Corner, (b) Surface Vertical Displacement, (c) Temperature-Induced Curl

estimate the effectiveness of numerous schemes for curling behavior mitigation.

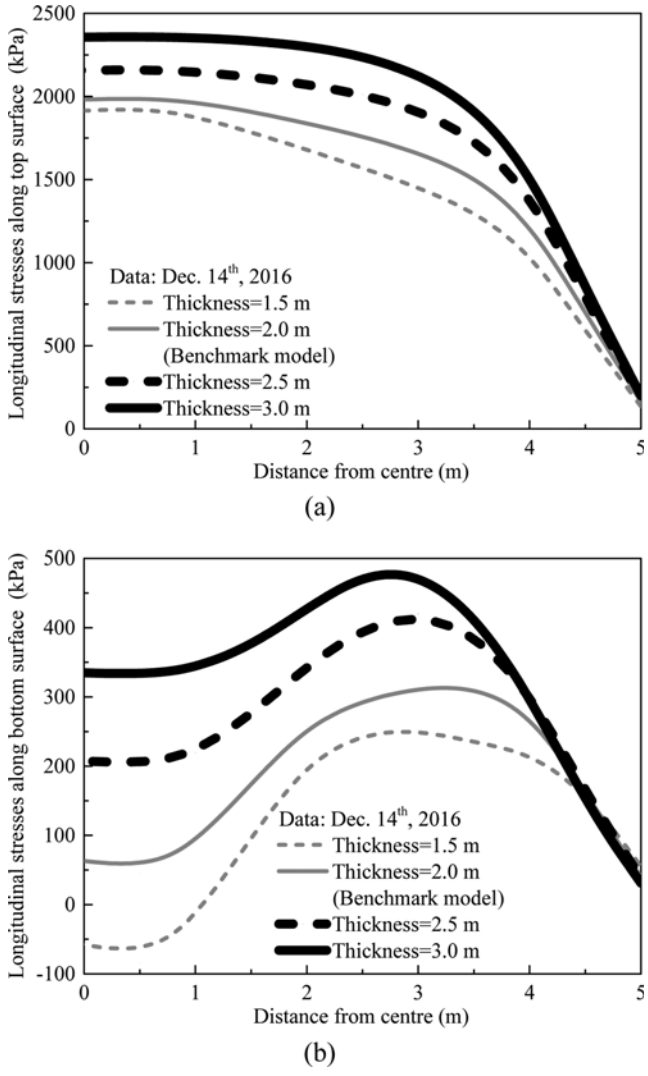

Fig. 10. Effect of Slab Thickness on the Longitudinal Stresses of the Concrete Roadbed: (a) Along Top Surface, (b) Along Bottom Surface

4.1 Effect of Changing the Concrete Roadbed Thickness

Figure 9(a) shows the corner vertical displacements, vertical surface displacements and curl time histories of the concrete roadbed. Mitigation by adjusting the roadbed thickness has side effects. The increased thickness of the concrete roadbed will mitigate the upward deformation and magnify the downward deformation of the corner. As shown in Fig. 9(a), the most significant upward-curling behavior occurs on December 14, 2016. The maximum vertical surface displacement is shown in Fig. 9(b), and the distances of 0 m and 5 m correspond to the center and the corner, respectively. A similar slope of the curves is attained within various concrete roadbeds. Moreover, the lower thickness resulted in larger upward-curling behavior and slighter downward-curling behavior.

Figures 10(a) – 10(b) illustrates the influence of slab thickness on the longitudinal stress distributions in the top and bottom of the slab. The FE analysis results show that the top surface of the slab

is in tension. The tensile stresses at the corner of the top surface are approximately equal among different thicknesses, and the tensile stresses increase as the thickness increases in other locations. As shown in Fig. 10(b), the middle of the bottom is compressive when the thickness is greater than 3 m. The location of the maximum tensile stresses at the bottom is approximately 2 m away from the corner.

4.2 Effect of Changing the Concrete Roadbed Length

Figures 11(a) – 11(c) illustrates the variations in deformation behavior for different slab lengths. As the curling behavior turns into an upward-curling condition, the equilibrium paths begin to diverge. As the length increases, the upward deformation of the corner increases. Moreover, the time for turning into the downward-curling condition is the same. Indeed, the variations in curling are very similar when the length is longer than 20 m.

In Figs. 12(a) – 12(b), the longitudinal stress diagrams for the top and bottom of the slab are presented for a range of slab lengths (10 m, 15 m, 20 m, 25 m, and 30 m). Considering only thermal loads, the minimum tensile stress in the top

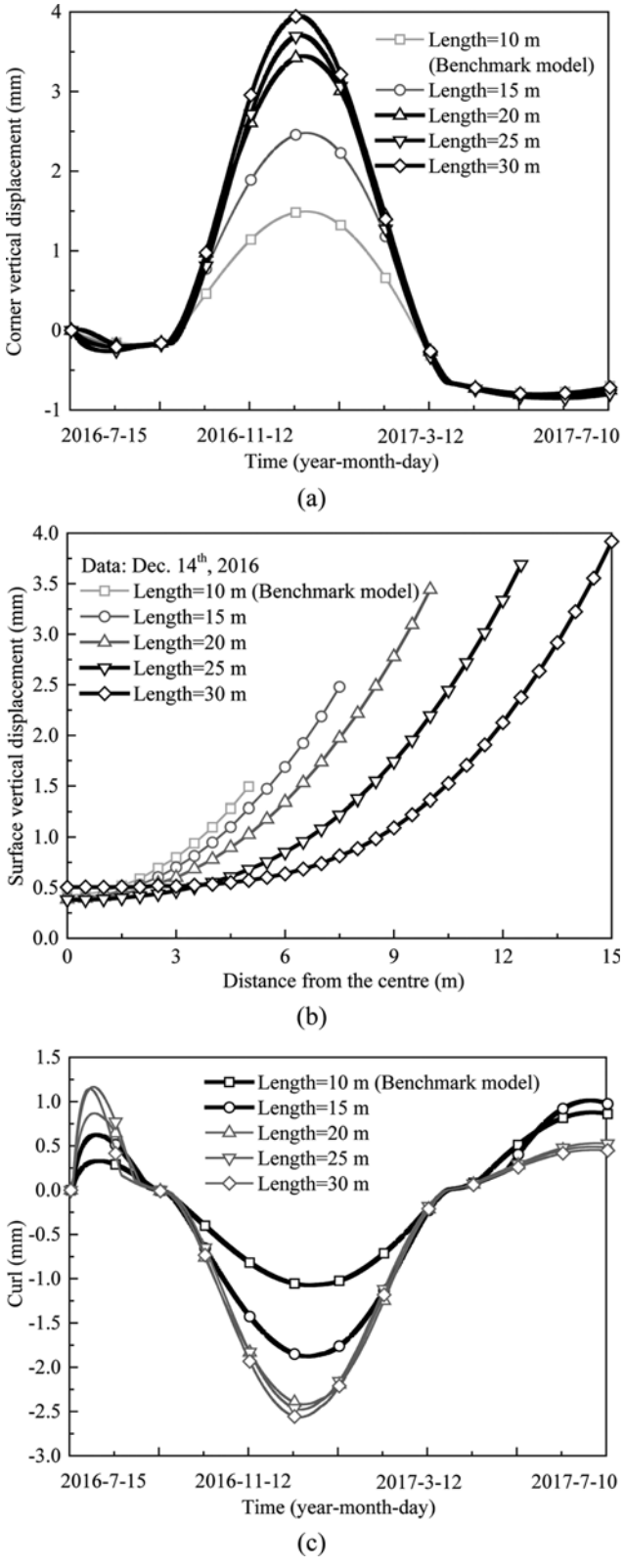

Fig. 11. Effect of Slab Length on the Deformation Behavior of the Concrete Roadbed: (a) Vertical Displacement at Roadbed Corner, (b) Surface Vertical Displacement, (c) Temperature-Induced Curl

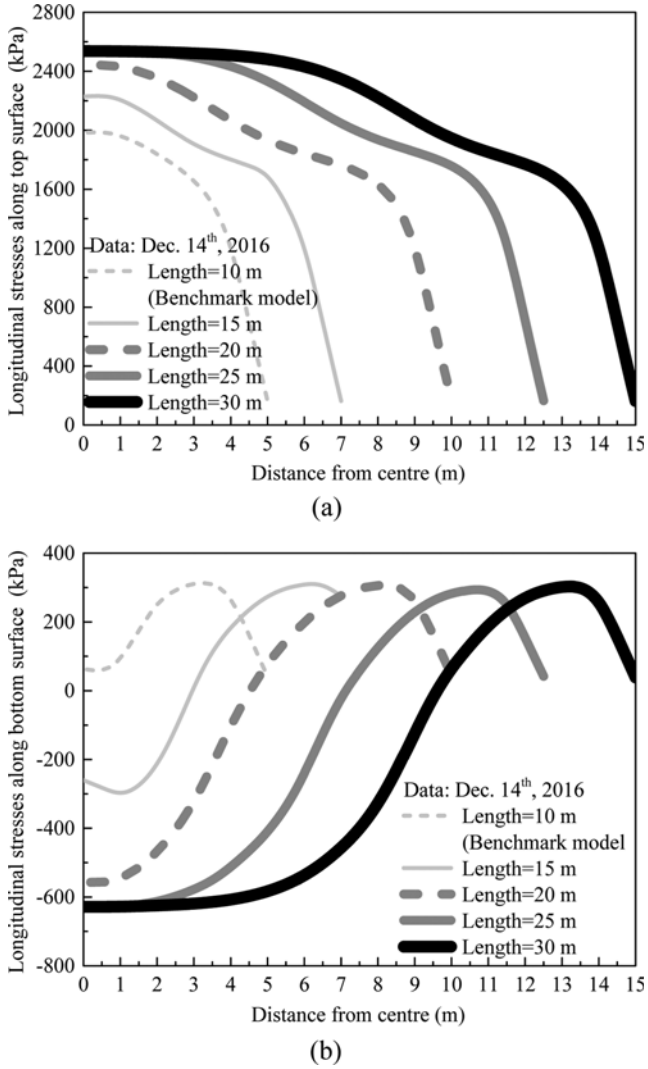

Fig. 12. Effect of Slab Length on the Longitudinal Stresses of the Concrete Roadbed: (a) Along Top Surface, (b) Along Bottom Surface

surface of the concrete roadbed occurs using the 10 m slab length. As the length increases, the tensile stress in the top surface increases. When the length is longer than 20 m, the tensile stresses in the middle of the top surface tend to converge. The same evolutionary law can be found in the middle of the bottom surface. When the length is longer than 10 m, the tensile stress in the middle of the bottom surface turns into compressive stress. It is noticeable that the maximum tensile stress in the bottom surface and its relative location is the same in the concrete roadbed with different lengths.

4.3 Effect of Setting Grooves on the Concrete Roadbed

For the real site conditions of the Beijing-Shenyang high-speed railway, it is economical and reasonable to construct a concrete roadbed with a 20 – 25 m concrete slab. From the discussion above, it is better to choose a concrete roadbed with a large thickness and short length. Thus, a concrete slab with a length of 20 m and thickness of 2.5 m is chosen as the mitigation object in this section. Then, a mitigation method can be

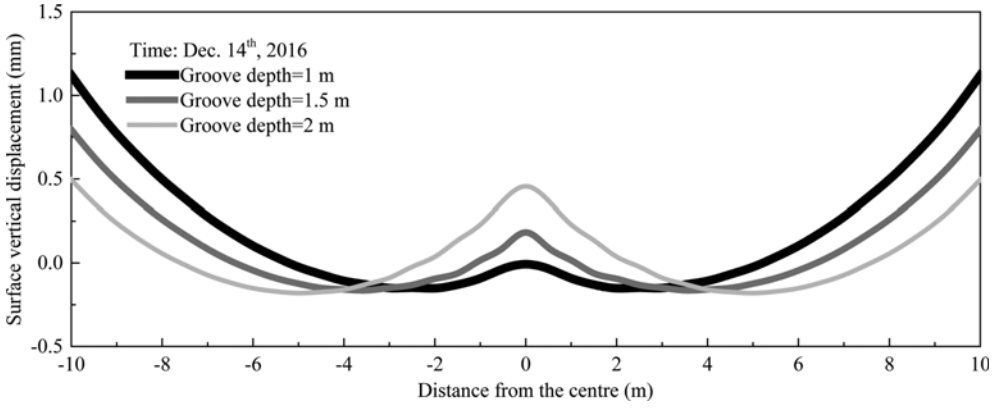

Fig. 13. Surface Vertical Displacement of Improved Concrete Roadbed with Various-Depth Single Groove

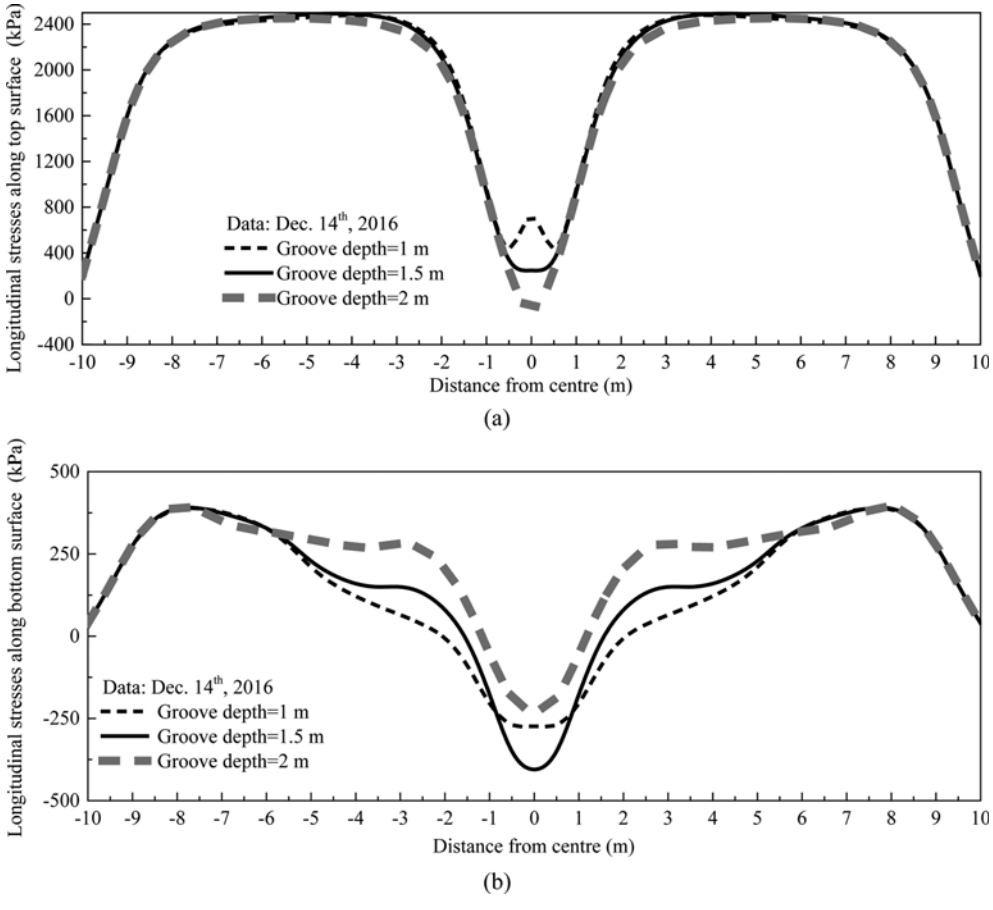

Fig. 14. Effect of Groove Depth on the Longitudinal Stresses of the Concrete Roadbed: (a) Along Top Surface, (b) Along Bottom Surface

provided by setting grooves on the concrete roadbed. The groove is parallel to the expansion joint with a width of 30 mm. In this section, the effects of different layout schemes of the groove are studied.

4.3.1 Mitigation Effect with a Single Groove

As shown in Fig. 13, the mitigation effect with a single groove is remarkable. When the groove depth is 2 m, the maximal vertical displacement of the roadbed with a single groove is only 0.5 mm. As the groove depth increases, the vertical displacement at the corner decreases, whereas the vertical displacement at the center increases. When the groove depth is 2 m, the vertical displacements at the corner and the center are similar.

In Fig. 14(a), the longitudinal stress diagrams for the top of the slab with a single groove are presented. Beyond the affected area of 1 m around the groove, changing the groove depth has no influence on the tensile stress on the top surface of the concrete roadbed. The center of the top surface is in compression when the groove depth is 2 m. By comparison, a groove depth of 1.5 m is conducive to the service properties of the center of the concrete roadbed.

Figure 14(b) illustrates the influence of the groove depth on the longitudinal stress distributions of the bottom of slab. The affected area described above increases to 6 m around the groove, and the groove depth can influence the range of the in-compression area. As the depth of the groove increases, the range of the in-compression area of the bottom surface decreases. The fluctuations in the longitudinal stress distributions are smaller for the concrete roadbed with a 2 m depth-groove.

To find a better mitigation method, this study analyzes the effect of groove width on the performance of the mitigation method. Fig. 15 indicates that the groove width has a statistically insignificant influence on the temperature-induced curl of the improved concrete roadbed. Additionally, the horizontal movement of the groove side is smaller than 5 mm for all cases. Therefore, there is no self-restraining effect.

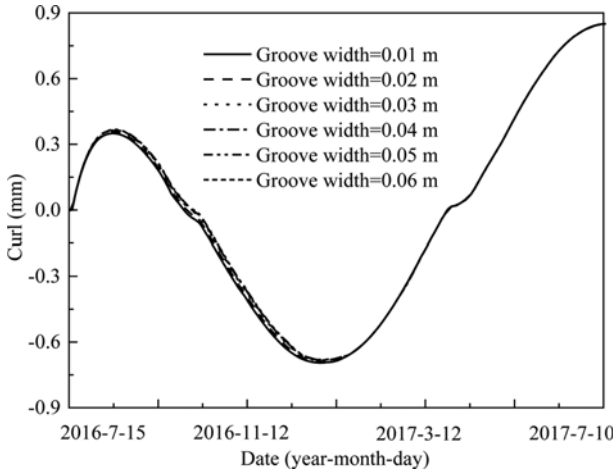

Fig. 15. Temperature-Induced Curl of Improved Concrete Roadbed with Various-Width Single Groove

4.3.2 Mitigation Effect with a Double Groove

To compare the mitigation effect of the double groove method with the single groove method, the same mitigation object described above is chosen in this section. Considering the fixed width (8.9 m) of the concrete roadbed and the fixed length of the CRTS-II slab track, two types of segment length ratios (short: long: short and long: short: long) are chosen to analyze the mitigation effect with double grooves (depth = 2 m).

The FE analysis results in Fig. 16 show that the double groove method of both types exhibit 50% lower maximal vertical roadbed displacement than the corresponding single groove method. However, for two different adjacent segments in a roadbed, as the difference in length increases, the difference in vertical displacement between the corner and the groove side increases. This discrepancy will affect the uniformity of the roadbed. Thus, it is preferable to place the longer segment between two shorter segments, as the vertical displacement at the corner and the groove side can be adjusted to be consistent.

As shown in Fig. 17, for the type 1 double groove method, the maximum longitudinal tensile stress in both the top and bottom

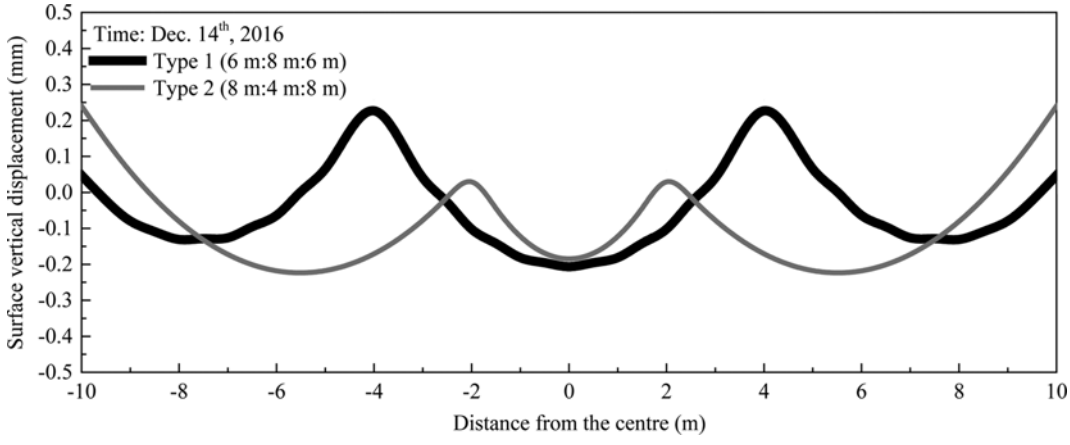

Fig. 16. Surface Vertical Displacement of Improved Concrete Roadbed with Various-Depth Double Groove

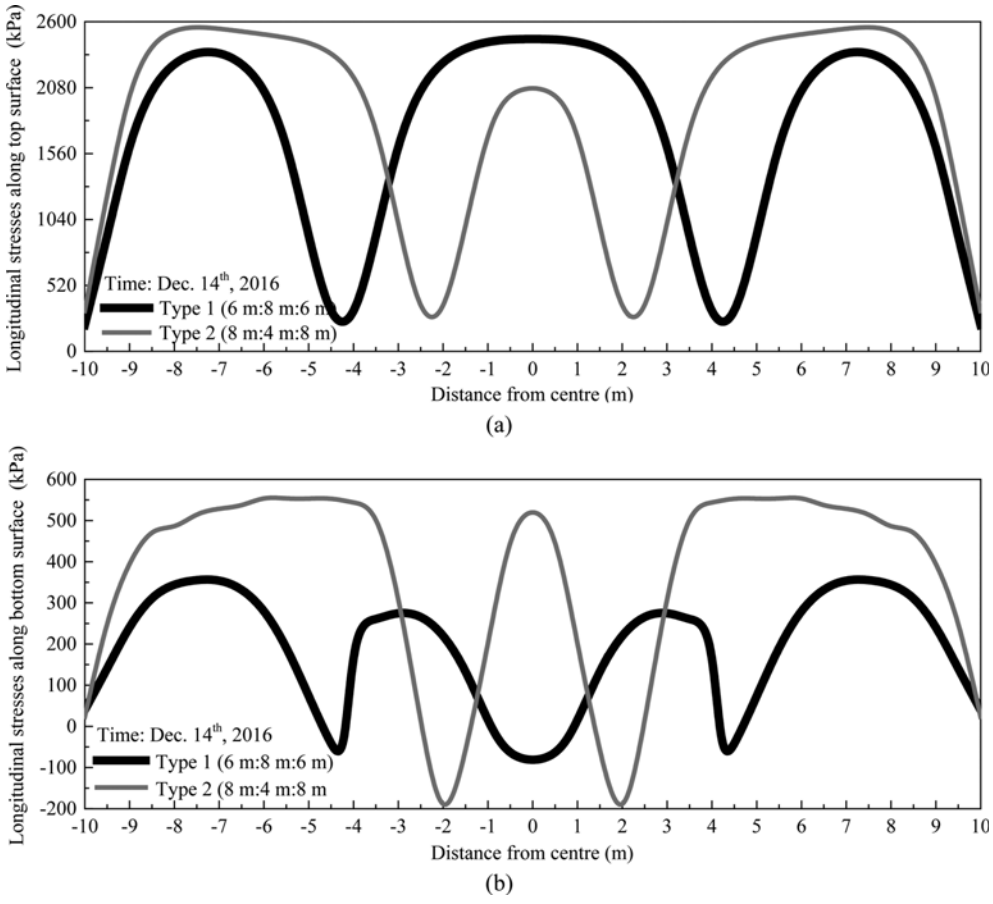

Fig. 17. Effect of Slab Thickness on the Longitudinal Stresses of the Concrete Roadbed: (a) Along Top Surface, (b) Along Bottom Surface

surface decreases relative to that in the single groove method. For the 8 m segment, the longitudinal stress in both the top and bottom surfaces in type 1 is smaller than that in type 2. The middle area in the bottom surface of type 2 is in severe tension, which is dangerous for the concrete roadbed.

5. Conclusions

In this study, the temperature field and the curling behavior of concrete roadbeds are characterized by in situ monitoring experiments. On the basis, a series of parametric studies are conducted focusing mainly on the influence of mitigation measures on the temperature-induced curling behavior. The main findings from this study are as follows:

1. A longer concrete roadbed has a greater fluctuation in the vertical corner movement and a greater upward-curling behavior under the same environmental conditions. But, the variation in curling behavior is very similar when the length is longer than 20 m. Meanwhile, mitigating the upward-curling behavior by adjusting the thickness will result in severe downward-curling behavior.
2. For the single groove mitigation method, as the depth of the groove increases, the range of the in-compression area of the bottom surface decreases, and the observed fluctuations in the longitudinal stress distributions are smaller. Beyond the affected area of 1 m around the groove, changing the groove depth has no influence on the tensile stress on the top surface of the concrete roadbed.
3. For the double groove mitigation method with different groove locations, it is preferable to place the longer segment between two shorter segments, as the vertical displacement at the corner and the groove side can be adjusted to be consistent. Otherwise, the middle area in the bottom surface may be in severe tension.

Acknowledgements

This research was supported by the National Key R&D Program of China (Grant No. 2016YEE0205100), the Key Program of the National Natural Science Foundation of China (Grant No. 41430634), the National Major Scientific Instruments Development Project of China (Grant Nos. 41627801 and 41702382), the Open Research Fund Program of the State Key Laboratory for Geomechanics and Deep Underground Engineering of China (Grant No. SKLGDUEK1807), the Open Research Fund Program of the State Key Laboratory of Permafrost Engineering of China (Grant No. SKLFSE201709), the Opening Fund for Innovation Platform of China (Grant No. 2016YJ004), and the Technology

Research and Development Plan Program of China Railway Corporation (Grant No. 2016G002-F).

Nomenclature

A = temperature amplitude at the natural ground surface
t = time
T_n = surface boundary temperature
T_a = ground surface mean temperature
α_0 = initial phase angle
ΔT_F = temperature increment caused by adherent layer
ΔT_g = temperature gradient
ΔT_w = temperature increment caused by climate warming effect
δ = vertical deflections

ORCID

Yuan Yu https://orcid.org/0000-0001-5898-7301
Liang Tang https://orcid.org/0000-0003-0030-1850
Xianzhang Ling https://orcid.org/0000-0002-0384-9232
Degou Cai https://orcid.org/0000-0002-9558-7937
Yangsheng Ye https://orcid.org/0000-0001-9970-7943
Lin Geng https://orcid.org/0000-0001-6403-1672

References

ABAQUS (2013) User's manual. Dassault Systèmes Simulia Corp., Providence, RI, USA

Al Nasra M, Wang LRL (1994) Parametric study of slab-on-grade problems due to initial warping and point loads. *ACI Structural Journal* 91(2):198-210, DOI: 10.14359/4596

Armaghani JM, Larsen TJ, Smith LL (1987) Temperature response of concrete pavements. *Transportation Research Board* 1121:23-33

Beckemeyer C, Khazanovich L, Yu T (2002) Determining amount of built-in curling in jointed plain concrete pavement: Case study of Pennsylvania 1-80. *Transportation Research Record* 1809:85-92, DOI: 10.3141/1809-10

Bianchini A (2013) Evaluation of temperature-induced curling in concrete slabs using deflection difference analysis. *Journal of Transportation Engineering* 139(2):130-137, DOI: 10.1061/(ASCE)TE.1943-5436.0000490

Byrum CR (2000) Analysis by high-speed profile of jointed concrete pavement slab curvatures. *Transportation Research Board* 1730(1):1-9, DOI: 10.3141/1730-01

Canakci H, Hamed M, Celik F, Sidik W, Eviz F (2016) Friction characteristics of organic soil with construction materials. *Soils and Foundations* 56(6):965-972, DOI: 10.1016/j.sandf.2016.11.002

Canga Ruiz AE, Qian Y, Edwards JR, Dersch MS (2019) Analysis of the temperature effect on concrete crosstie flexural behavior. *Construction and Building Materials* 196:362-374, DOI: 10.1016/j.conbuildmat.2018.11.065

Genikomsou AS, Polak MA (2015) Finite element analysis of punching shear of concrete slabs using damaged plasticity model in ABAQUS. *Engineering Structures* 98:38-48, DOI: 10.1016/j.engstruct.2015.04.016

Hansen W, Smiley DL, Peng YF, Jensen EA (2002) Validating top-down premature transverse slab cracking in jointed plain concrete pavement. *Transportation Research Record* 1809(1):52-59, DOI: 10.3141/1809-06

Jeong JH, Park JY, Lim JS, Kim SH (2014) Testing and modelling of friction characteristics between concrete slab and subbase layers. *Road Materials and Pavement Design* 15(1):114-130, DOI: 10.1080/14680629.2013.863161

Lee J, Fenves GL (1998) A plastic-damage concrete model for earthquake analysis of dams. *Earthquake Engineering and Structural Dynamics* 27(9):937-956, DOI: 10.1002/(sici)1096-9845(199809)27:9<937::Aid-eqe764>3.0.Co;2-5

Leonards GA, Harr ME (1959) Analysis of concrete slabs on ground. *Journal of the Soil Mechanics and Foundations Division* 85(3):35-58

Lubliner J, Oliver J, Oller S, Oñate E (1989) A plastic-damage model for concrete. *International Journal of Solids and Structures* 25(3):299-326, DOI: 10.1016/0020-7683(89)90050-4

Mackiewicz P (2014) Thermal stress analysis of jointed plane in concrete pavements. *Applied Thermal Engineering* 73(1):1169-1176, DOI: 10.1016/j.applthermaleng.2014.09.006

Mirza O, Kaewunruen S, Dinh C, Pervanic E (2016) Numerical investigation into thermal load responses of railway transom bridge. *Engineering Failure Analysis* 60:280-295, DOI: 10.1016/j.engfailanal.2015.11.054

Mohamed AR, Hansen W (1997) Effect of nonlinear temperature gradient on curling stress in concrete pavements. *Transportation Research Record* 1568(1):65-71, DOI: 10.3141/1568-08

Mohamad ME, Ibrahim IS, Abdullah R, Abd Rahman AB, Kueh ABH, Usman J (2015) Friction and cohesion coefficients of composite concrete-to-concrete bond. *Cement and Concrete Composites* 56:1-14, DOI: 10.1016/j.cemconcomp.2014.10.003

Nam BH, Yeon JH, Behring Z (2014) Effect of daily temperature variations on the continuous deflection profiles of airfield jointed concrete pavements. *Construction and Building Materials* 73:261-270, DOI: 10.1016/j.conbuildmat.2014.09.073

Rao S, Roesler JR (2005) Characterizing effective built-in curling from concrete pavement field measurements. *Journal of Transportation Engineering* 131(4):320-327, DOI: 10.1061/(ASCE)0733-947X(2005)131:4(320)

Ren JJ, Yang RS, Wang P, Yong P, Wen C (2014) Slab upwarping of twin-block slab track on subgrade-bridge transition section: parameter study and repair method. *Transportation Research Record* 2448(1):115-124, DOI: 10.3141/2448-14

Sabih G, Tarefder RA (2016) Impact of variability of mechanical and thermal properties of concrete on predicted performance of jointed plain concrete pavements. *International Journal of Pavement Research and Technology* 9(6):436-444, DOI: 10.1016/j.ijprt.2016.09.005

Suprenant BA (2002) Why slabs curl, Part II: Factors affecting the amount of curling. *Concrete International* 24(4):59-64

TB 10621 (2014) Code for design of high speed railway. China Railway Publishing House, Beijing, China (in Chinese)

Wei Z, Jin HJ, Zhang JM, Yu SP, Han XJ, Ji YJ, He RX, Chang XL (2011) Prediction of permafrost changes in Northeastern China under a changing climate. *Science China Earth Sciences* 54(6):924-935, DOI: 10.1007/s11430-010-4109-6

Wolf HE, Qian Y, Edwards JR, Dersch MS, Lange DA (2016) Temperature-induced curl behavior of prestressed concrete and its effect on railroad crossties. *Construction and Building Materials* 115:319-326, DOI: 10.1016/j.conbuildmat.2016.04.039

Yang GT, Bradford MA (2017) A refined modelling for thermal-induced upheaval buckling of continuously reinforced concrete pavements. *Engineering Structures* 150:256-270, DOI: 10.1016/j.engstruct.2017.06.005

Yu HT, Khazanovich L, Darter MI, Ardani A (1998) Analysis of concrete pavement responses to temperature and wheel loads measured from intrumented slabs. *Transportation Research Record* 1639(1):94-101, DOI: 10.3141/1639-10

Zhu SY, Cai CB (2014) Interface damage and its effect on vibrations of slab track under temperature and vehicle dynamic loads. *International Journal of Non-Linear Mechanics* 58:222-232, DOI: 10.1016/j.ijnonlinmec.2013.10.004